Indirect estimation of soil thermal properties and water flux using heat pulse probe measurements: Geometry and dispersion effects

Jan W. Hopmans
Department of Land, Air and Water Resources, University of California, Davis, California, USA

Jirka Šimunek
George E. Brown Jr. Salinity Laboratory, Agricultural Research Service, U.S. Department of Agriculture, Riverside, California, USA

Keith L. Bristow
CSIRO Land and Water, Townsville, Queensland, Australia

Received 6 November 2000; revised 24 August 2001; accepted 24 September 2001; published 29 January 2002.

[1] Traditionally, analytical solutions for heat transport in soils have been used in combination with heat pulse probe (HPP) measurements to estimate soil thermal properties. Although the analytical method has resulted in accurate estimation of soil thermal properties, we suggest that parameter estimation using inverse modeling (IM) provides new and unique opportunities for soil thermal characterization. Moreover, we show that the IM approach provides accurate estimation of soil water flux density in both unsaturated and saturated soil conditions for a wider range of water velocities than originally thought possible. Specifically, we show that accurate soil water velocity is obtained, simultaneously with soil thermal properties, if heat dispersion is included in the heat transport equation. The requirement for including heat dispersivity depends on the value of the newly defined dimensionless Keith Jirka Jan (KJJ) number, which is equal to the ratio of thermal dispersion to thermal conductivity. For example, when KJJ > 1, ignoring thermal dispersivity leads to errors in the water flux density which can exceed 10%. By including thermal dispersivity, water flow velocities were accurately determined for water flux densities ranging from 1.0 to >10 m d^{-1}. We also demonstrate the general application of inverse modeling to estimate soil thermal properties and their functional dependence on volumetric water content in a separate numerical experiment. We suggest that inverse modeling of HPP temperature data may allow simultaneous estimation of soil water retention (when combined with matric potential measurements) and unsaturated hydraulic conductivity (through water flux estimation) from simple laboratory experiments. *INDEX TERMS:* 1866 Hydrology: Soil moisture; 1875 Hydrology: Unsaturated zone; 1894 Hydrology: Instruments and techniques; *KEYWORDS:* Soil water flow; soil heat flow; inverse modeling; dispersivity

1. Introduction

[2] In the past decade, soil thermal research has advanced development of the heat pulse technique for estimation of soil thermal properties, i.e., soil thermal conductivity (λ), volumetric heat capacity (C), and soil thermal diffusivity (κ). Apart from needing to characterize the soil's physical properties, knowledge of the soil thermal properties is required for accurate prediction of soil temperature and its influence on seed emergence and crop growth [e.g., *Gilmore and Rogers*, 1958], soil water retention and unsaturated hydraulic conductivity [*Hopmans and Dane*, 1986b], and soil water vapor flow [*Nassar and Horton*, 1992] in coupled water and heat transport. It is expected that interest in the soil thermal regime will become increasingly important as both fundamental and applied research questions are posed regarding the water movement in radioactive waste repositories [*Tsang and Pruess*, 1987] and the fate and transport of high vapor pressure liquids (e.g., solvents) and microbes (e.g., bacteria and viruses). In addition, many chemical processes in soils are temperature-dependent, and their functioning in contaminant transport requires better prediction of soil temperature regimes.

[3] The soil thermal properties can be quickly and conveniently measured using heat pulse probes [*Campbell et al.*, 1991; *Bristow et al.*, 1993, 1994a, 1994b]. The dual probe consists of thin needle-like heater and temperature probes (~1-mm outer diameter), which are mounted in parallel with a 6-mm separation distance. A heat pulse is applied to the linear heater, and the temperature response is recorded at the sensor probe. *Campbell et al.* [1991] presented the analytical solution for the temperature rise of an instantaneous heat pulse, allowing estimation of the soil's volumetric heat capacity and volumetric water content if some additional data are available. Subsequently, *Bristow et al.* [1993] extended the probe to three needles to correct for drift in background temperature. Furthermore, they emphasized the relatively large sensitivity of water content estimations to error in the heater-sensor spacing (r). Continued development of radial heat transport theory resulted in application of the heat pulse probe (HPP) method to simultaneously estimate the soil's volumetric heat capacity and thermal conductivity (and hence thermal diffusivity) as well as water content, using a short-duration heat pulse from an infinite line source [*Bristow*, 1998]. Error analyses by *Kluitenberg et al.* [1993] for the instantaneous heat pulse and by *Kluitenberg et al.* [1995] for the short-duration heat

0043-1397/02/2000WR000071$09.00

pulse technique highlighted the importance of accurate r and time-to-maximum (t_{max}) temperature rise measurements on the accuracy of the thermal and water content estimations. It was determined that rigid needles are required to minimize changes in mutual probe positions while inserting the heat pulse probe into soils. Typical heat pulse strengths used for making HPP measurements cause a temperature rise of $\sim$1°C at the sensing probe, so that a 5% precision in heat capacity estimation requires temperature measurements with $\sim$0.05°C precision [*Kluitenberg et al.*, 1993].

[4] Further developments have led to the simultaneous measurement of soil thermal properties, water content, and electrical conductivity using TDR time domain reflectometry (TDR) combined with the HPP [*Noborio et al.*, 1996; *Ren et al.*, 1999]. *Bristow et al.* [2001] showed that a simple modification of the dual probe with an additional two needles for bulk soil electrical conductivity measurements provides an alternative measure of the soil's electrical conductivity. In a subsequent study, *Ren et al.* [2000] reported on the possibility of using a three-needle heat pulse probe to indirectly estimate water flux density from temperature responses, measured upstream and downstream of the heat source. Their experimental results, using the maximum difference between the upstream and downstream temperature signals (MDTD), indicated that such analysis can be successful for flux density values larger than 10^{-5} m s^{-1} (0.864 m d^{-1}). However, their results also suggested that the method is limited at higher fluxes (larger than $\sim$2.4 m d^{-1}), because of a systematic overestimation of MDTD by 10% or more at these higher water velocities. The discrepancy may be the result of ignoring the finite heater geometry in the heat analysis, which assumes infinitely small point sources and sensors with negligible diameter. Although not important for zero-water flow conditions [*Kluitenberg et al.*, 1995], it could be an important consideration when using the HPP for estimation of water flux. Moreover, the finite physical size of the needles may distort the water flow field between the needles, thereby affecting effective flow of water and heat between the heat source and sensor. Although the proposed flux density measurement of *Ren et al.* [2000] requires a priori knowledge of the thermal properties, these can be obtained separately from zero-water flux heat probe measurements, using the method of *Bristow et al.* [1994a]. Also, *Ren et al.* [2000] suggested that the limit of sensitivity could be lowered to $\sim 10^{-6}$ m s^{-1} (0.0864 m d^{-1}) if the temperature measurement precision is 0.01°C. It is expected that even lower water velocities can be measured for unsaturated soils because of the reduction in the bulk soil heat capacity with decreasing water content.

[5] In this paper, we hypothesize that difficulties in using the HPP for water flux density measurements is partly caused by the omission of dispersive heat transport in the heat flow equation. As solute dispersion is generally important for solute transport in soils, thermal dispersion should also be considered for heat transport. For solute transport, molecular diffusion and hydrodynamic dispersion combined make up the soil's dispersion coefficient. By analogy, the effective thermal conductivity (λ_{eff}) is the sum of the bulk soil thermal conductivity with stationary fluids (λ_0) and a kinematic thermal dispersion term (λ_d), resulting from the heterogeneity of water velocities within and between water-filled soil pores, to be defined later. It is expected that the influence of the additional dispersion term on heat transport in soils is most significant only at high water velocities, since it is only then that the thermal dispersion term is of the same order of magnitude or larger than the conductive term.

[6] If indeed successful, the multineedle heat pulse technique might be an essential new tool for general flow and transport studies in both the laboratory and the field because of its simple, accurate, and versatile design. Moreover, it is becoming increasingly clear that multifunctioning sensors are critical for accurate in situ soil physical measurements [*Hopmans et al.*, 1999] because of inherent soil spatial variability. In particular, we also note the promise of using inverse methodologies [*Hopmans et al.*, 2002] to infer in situ soil hydraulic, thermal, and solute transport characteristics and the possibilities of combining inverse modeling with multineedle heat pulse probe measurements.

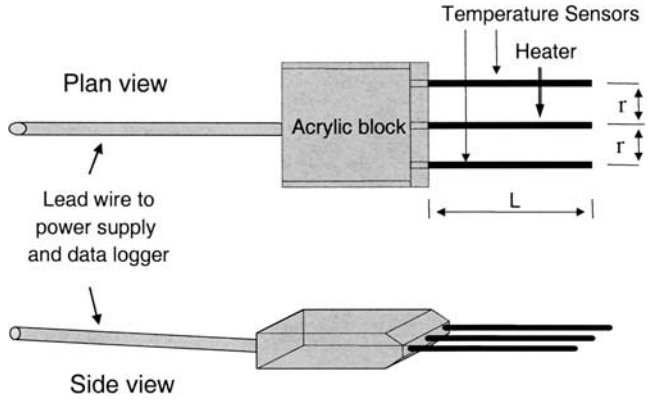

Figure 1. Schematic showing the heat pulse probe (HPP). The distance L = 30 mm in this particular case.

[7] The objective of this paper is therefore threefold. First, we provide a sensitivity analysis to illustrate the effect of the finite heat source needle on the temperature response for a range of water flux densities in both saturated and unsaturated soil conditions. We also use these data to demonstrate the effect of the finite probe geometry on inverse modeling estimation of water flux and thermal diffusivity. Second, in an additional sensitivity analysis we show the influence of thermal dispersion on heat transport and on the estimation of thermal properties and water flow density using parameter estimation by inverse modeling. The results suggest an alternative experimental design for the HPP that will provide more accurate water flux density measurements, even at high water velocities. Finally, the third objective is to evaluate the inverse modeling method for accurate estimation of soil water content, water flux density, and the water content dependence of soil thermal properties from HPP measurements.

2. Materials and Methods

2.1. Heat Pulse Probe (HPP)

[8] The theory assumes that the soil around the HPP is homogeneous and isotropic and that contact resistance between the soil and the probe needles is negligible. Moreover, it is assumed that the sensor needle has an infinitely small heat capacity and large thermal conductivity, so that temperature measurements are instantaneous. Typical heat pulse strengths and heat pulse durations are 480 J m^{-1} and 8s, respectively, so that the total quantity of heat released is $\sim$60 J m^{-1} s^{-1}. The assumed distance between the centers of the heater and sensor needles (r) is 6 mm, whereas the outside diameter of both needles is 1 mm. This basic structure depicted in Figure 1 with a needle length (L) of 30 mm agrees with the recommended dimensions as outlined by *Bristow et al.* [1994a, 2001]. The diagram in Figure 2 shows the physical dimensions of the simulated two-dimensional soil domain with the three-needle heat pulse probe (heater with upstream (U) and downstream (D) thermocouple) and includes an additional thermocouple location (T), which is transverse to the principal water flow direction. Later, we will suggest that

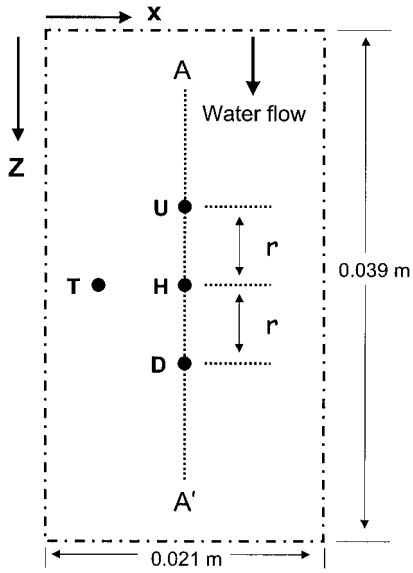

Figure 2. Simulated soil domain showing front view of heater needle (H), downstream (D), upstream (U), and transverse (T) sensors. Water flow direction is downstream.

additional temperature information from this transverse sensor needle will allow estimation of high water flow velocities. The HPP extends perpendicularly to the illustrated (x-z) plane of the soil domain, so that the HPP needles are represented by their cross-sectional circular planes within the vertical plane.

2.2. Thermal Properties

[9] The soil volumetric heat capacity, $C_{\text{bulk}} = (\rho c)_{\text{bulk}}$ (J m^{-3} K^{-1}), can be determined from the sum of the heat capacities of the individual constituents according to [*de Vries*, 1963]

$$C_{\text{bulk}} = (\rho c)_s(1-\phi) + (\rho c)_w\theta + (\rho c)_a(\phi-\theta), \tag{1}$$

where ρ is the density (kg m^{-3}), c is the specific heat (J kg^{-1} K^{-1}), ϕ is the porosity (m^3 m^{-3}), θ is the volumetric water content (m^3 m^{-3}), and the subscripts s, w, and a indicate the soil's solid phase, water, and air, respectively. If the heat capacity of air is ignored and the solid phase includes both mineral and organic matter fractions, setting $C_w = (\rho c)_w$ and $C_s = (\rho c)_s$ allows (1) to be rewritten as [*Campbell*, 1985]

$$C_{\text{bulk}} = C_s(1-\phi) + C_w\theta. \tag{2}$$

It is clear from (2) that the volumetric water content can be computed directly if C_{bulk} is measured using the HPP method and volumetric heat capacity values of the solid phase and water are known.

[10] The bulk soil thermal conductivity (λ_0) is a function of mineral type and geometrical arrangement of the various phases, as well as the water content [*de Vries*, 1963], and hence is soil specific. Although various empirical relationships have been suggested (including those by *Campbell* [1985], a three-parameter polynomial expression can be used for the water content range beyond the initial sharp increase in thermal conductivity with water content. This relationship is [*Chung and Horton*, 1987]

$$\lambda_0 = b_0 + b_1\theta + b_2\theta^{0.5}, \tag{3}$$

where b_0, b_1, and b_2 are empirical constants.

[11] In addition, the HPP method [*Bristow et al.*, 1994a] allows easy estimation of the thermal diffusivity κ (m^2 s^{-1}) from the thermal conductivity λ_0 (W m^{-1} K^{-1}) and volumetric heat capacity C_{bulk} (J m^{-3} K^{-1}) using

$$\kappa = \lambda_0 / C_{\text{bulk}}. \tag{4}$$

2.3. Heat Transport Equation

[12] The general two-dimensional heat transport equation for a homogeneous porous medium can be written as [*Bear*, 1972; *Sophocleous*, 1979; *Šimunek et al.*, 1999]

$$C_{\text{bulk}}(\theta)\frac{\partial T}{\partial t} = \frac{\partial}{\partial x_i}\left[\boldsymbol{\lambda}_{\text{eff},ij}(\theta)\frac{\partial T}{\partial x_j}\right] - C_w q_{w,i}\frac{\partial T}{\partial x_i}, \tag{5}$$

where the subcript ij denotes the Einstein notation, T is temperature, and $\boldsymbol{\lambda}_{\text{eff},ij}$ is a second-order tensor of the effective thermal conductivity. The first term on the right-hand side represents heat flow due to conduction, whereas the second term accounts for convective heat transport by water flow as controlled by the water flux density $q_{w,i}$. This formulation assumes instantaneous heat transfer between phases, so that at any point in the bulk soil the solid, liquid, and gas temperatures are identical. For an isotropic porous medium the effective thermal conductivity can be written as [*De Marsily*, 1986; *Bear*, 1972]:

$$\boldsymbol{\lambda}_{\text{eff},ij}(\theta) = \lambda_0(\theta)\delta_{ij} + \delta_{ij}\beta_T C_w|q_w| + (\beta_L - \beta_T)C_w\frac{q_{w,j}\,q_{w,i}}{|q_w|} \tag{6}$$

to include the effect of hydrodynamic dispersion on heat transport. In analogy with solute transport, velocity variations within the water-filled pore spaces cause mixing of pore waters with different velocities, thereby causing dispersion-like properties of the temperature field. In (6), $|q_w|$ denotes the magnitude of the Darcy flux density, δ_{ij} is the Kronecker delta ($\delta_{ij} = 1$ if $i = j$ and $\delta_{ij} = 0$ if $i \neq j$), and β_L and β_T are the longitudinal and transverse heat dispersivities (m), respectively. In principle, their values should be of similar magnitude to the dispersivities defined for solute transport [*De Marsily*, 1986], but there is currently little information about their relationship. For water flow conditions where flow is uniform and parallel to the z axis, (6) can be simplified to

$$\lambda_{\text{eff},zz} = \lambda_0 + \lambda_{d,L} \qquad \lambda_{\text{eff},xx} = \lambda_0 + \lambda_{d,T}, \tag{7}$$

where $\lambda_{d,L} = \beta_L C_w q_{w,z}$ and $\lambda_{d,T} = \beta_T C_w q_{w,z}$ denote the longitudinal and transversal thermal dispersion coefficients, respectively. If the water flux density is zero, the convective term disappears and λ_{eff} equals the bulk soil thermal conductivity λ_0. While applying (7), it must be realized that the bulk soil thermal conductivity is relatively large so that dispersive effects on λ_{eff} may be small except for large water velocity values. To quantify the contribution of hydrodynamic dispersion, relative to the thermal conductivity (λ_0), we define the dimensionless Keith Jirka Jan (KJJ) number:

$$\text{KJJ} = \lambda_{d,L}/\lambda_0, \tag{8}$$

which is equal to one when the thermal dispersion is equal to the bulk soil thermal conductivity (λ_0).

[13] For uniform vertical water flow conditions the simplified heat flow equation, after dividing the left-and right-hand side of (5) by C_{bulk}, can be written as

$$\frac{\partial T}{\partial t} = \frac{\partial}{\partial x}\left[\kappa_{xx}\frac{\partial T}{\partial x}\right] + \frac{\partial}{\partial z}\left[\kappa_{zz}\frac{\partial T}{\partial z}\right] - \left[V_h\frac{\partial T}{\partial z}\right], \tag{9}$$

where κ_{xx} and κ_{zz} denote the effective thermal diffusivity in the x and z direction, respectively, defined by

$$\kappa_{xx}(\theta) = \frac{\lambda_0(\theta) + \lambda_{d,T}(q_{w,z})}{C_{\text{bulk}}(\theta)} \qquad \kappa_{zz}(\theta) = \frac{\lambda_0(\theta) + \lambda_{d,L}(q_{w,z})}{C_{\text{bulk}}(\theta)} \tag{10}$$

and where

$$V_h = \frac{C_w q_{w,z}}{C_{\text{bulk}}} = \frac{\theta C_w V_w}{C_{\text{bulk}}} \tag{11}$$

denotes the convective heat pulse velocity, describing heat flow by the moving liquid phase, relative to the stationary bulk porous medium [*Ren et al.*, 2000]. Since $(\theta C_w/C_{\text{bulk}}) < 1.0$ (from (2)), it follows that $V_h < V_w$, where V_w denotes the average pore water velocity. As pointed out by *Bear* [1972], the magnitude of convective relative to conductive heat transport can be summarized by the dimensionless Peclet number (*Pe*)

$$Pe = \frac{V_w \theta C_w d}{\lambda_{\text{eff}}} = \frac{V_h d}{K_{\text{eff}}}, \tag{12}$$

where d denotes the characteristic length of the porous medium (assumed to be equal to the mean grain size). The need to include dispersion in the bulk soil's thermal diffusivity will depend on the magnitude of the KJJ and Pe numbers, as hydrodynamic effects on heat transport may become significant at increasing pore water velocities.

2.4. Inverse Modeling

[14] Inverse modeling (IM) has been applied successfully mostly to the parameter estimation of soil water retention and unsaturated hydraulic conductivity functions. An extensive review of inverse modeling regarding parameter optimization is presented by *Hopmans et al.* [2002]. Using numerical simulations, soil hydraulic parameters can be determined for transient flow, so that IM can accommodate much more flexible experimental conditions than required for steady state methods for which analytical solutions are available. In the analysis to follow, we show how IM can be applied to coupled heat and water transport. Advantages of IM for analysis of the HPP measurements are the following: (1) Various parameters and/or variables can be estimated simultaneously (e.g., heat transport parameters and pore water velocity); (2) IM can be applied to coupled flow of heat and water, allowing optimization of both heat and water flow parameters; and (3) the number and type of measurements to achieve a well-posed solution is unlimited.

[15] The objective function Φ to be minimized during the parameter estimation process may be defined as

$$\phi(\mathbf{p}, T) = w_1 \sum_{i=1}^{n} [T^*(\mathbf{x}, t_i) - T(\mathbf{x}, t_i, \mathbf{p})]^2 + w_2[\Delta T^*_{ud}(t^*_{\max}) - \Delta T_{ud}(t^*_{\max}, \mathbf{p})]^2, \tag{13}$$

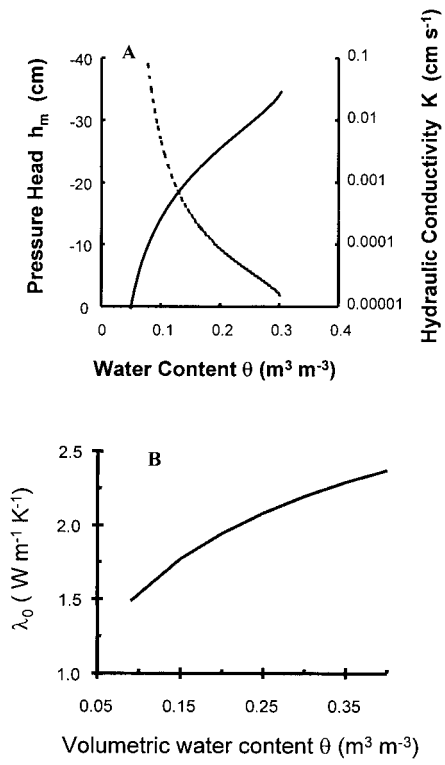

Figure 3. (a) Soil hydraulic functions (adapted from *Inoue et al.* [2000]) and (b) thermal conductivity function (adapted from *Chung and Horton* [1987]) for the Tottori sand.

where the right-hand side represents the residuals between the experimental (T^*) and corresponding predicted (T) temperatures. The vector $\mathbf{x}$ denotes the spatial coordinate of each measurement i, whereas the vector $\mathbf{p}$ contains the optimized parameters. The first term sums the residuals for all temperature measurements (n), whereas the second term provides the temperature difference between the upstream (u) and downstream (d) temperature measurement at time $t^* = t^*_{\max}$, where $t^*_{\max}$ is the time of the maximum temperature at the downstream sensor. Weighting factor values for w_1 and w_2 were set equal to one. The Levenberg-Marquardt (LM) method was used to minimized (13), thereby including computed confidence intervals for the optimized parameters, assuming zero model error. For the sensitivity analysis discussed in this paper, the ''experimental'' temperature data are provided by simulated data, using forward simulations with the same flow and transport code as used for the IM (HYDRUS-2D). The results of these types of studies will help in selecting optimum experimental conditions so that IM can be applied most effectively by yielding accurate and unique parameter values.

2.5. HYDRUS-2D Simulation Model

[16] The model environment selected for the sensitivity analysis of the HPP is the HYDRUS-2D code [*Šimunek et al.*, 1999], which incorporates transient simultaneous water and heat flow in two spatial dimensions (x and z) combined with LM optimization algorithm for parameter estimation using IM. The domain size was fixed to 0.025 m (horizontal) by 0.1 m (vertical) with a nodal spacing of 0.5 mm for the structured mesh used for the point heater needle (total of 10,000 elements) and a nodal spacing varying between 0.2 mm (near needles) and 3 mm (near domain boundaries) for the unstructured mesh (total of 1700 elements) used for the

Table 1. Soil Hydraulic and Thermal Properties Used in This Study

Parameter	Units	Value	Reference
θ_r	$m^3\ m^{-3}$	0.027	*Inoue et al.* [2000]
θ_s	$m^3\ m^{-3}$	0.310	
α	m^{-1}	13.8	
n	dimensionless	2.01	
K_s	$m\ s^{-1}$	0.00045	
l	dimensionless	−1.16	
β_L	m	0.00221	
β_T	m	0.1 β_L	*Šimunek et al.* [1999], *Bear* [1972]
d	mm	0.36	*Shiozawa and Inoue* [2001]
b_0	dimensionless	0.228	*Chung and Horton* [1987]
b_1	dimensionless	−2.406	
b_2	dimensionless	4.909	
C_w	$J\ m^{-3}\ K^{-1}$	4.18×10^6	
C_s[a]	$J\ m^{-3}\ K^{-1}$	1.92×10^6	

[a] $C_s = (\rho c)_s$, with c_s = 717 J kg^{-1} K^{-1} and ρ_s = 2650 kg m^{-3}.

other simulations that considered a finite size heater needle. The numerical analysis assumes that the temperature and needle probes extend infinitely in the y direction, perpendicular to the (x-z) plane of the simulated soil domain (Figure 2), thereby ignoring possible three-dimensional effects that may occur for finite HPP needles. The soil hydraulic properties for the Tottori sand used in the study are presented in Figure 3a [*Inoue et al.*, 2000], whereas the mean grain size (d) was taken from *Shiozawa and Inoue* [2001]. The functional dependence of thermal conductivity with water content (Figure 3b) for this sandy soil was taken from *Chung and Horton* [1987].

[17] To simplify the analysis, either steady state vertical water flow or no water flow was assumed. Hence water flux is governed by the Darcy flux q_w and is written for the respective z and x directions as

$$q_{w,z} = -K(h_m)\left(\frac{\partial h_m}{\partial z} + 1\right) \qquad q_{w,x} = -K(h_m)\left(\frac{\partial h_m}{\partial x}\right), \quad (14)$$

where K ($m\ s^{-1}$) denotes the unsaturated hydraulic conductivity and h_m (m) denotes the soil water matric potential. The flux in the x direction (transverse direction) is included for completeness, since some lateral flow will occur around the finite heater needle. Zero flux is imposed on the lateral boundaries of the soil domain (parallel with the main water flow direction), whereas the imposed steady state vertical water flux is controlled by water potential values at the horizontal boundaries of the simulated soil domain. The soil hydraulic properties are described by the van Genuchten (soil water retention) and van Genuchten-Mualem (unsaturated hydraulic conductivity) relationships [*Van Genuchten*, 1980]:

$$S_e = \frac{\theta - \theta_r}{\theta_s - \theta_r} = [1 + (\alpha|h_m|)^n]^{-m} \quad (15a)$$

$$K = K_s S_e^l \left[1 - \left(1 - S_e^{1/m}\right)^m\right]^2, \quad (15b)$$

where S_e is the effective saturation, θ_s, θ_r, and θ are saturated, residual, and actual water contents, respectively, α, n, and l are constants, $m = 1 - 1/n$, and K_s denotes the saturated hydraulic conductivity. Parameters for both the soil hydraulic and thermal properties are summarized in Table 1.

[18] Although HYDRUS-2D solves for both transient heat and water flow, their coupling is limited to the mutual occurrence of water flux density and water content in both transport equations. Simultaneous solution of both transport equations is done by first solving the water flow equation and by subsequent substitution of the computed flux density and water content values into the heat flow equation for each time step. However, temperature effects on soil hydraulic properties [*Hopmans and Dane*, 1986a] and thermal properties [*Hopmans and Dane*, 1986b] were ignored. Moreover, distillation effects causing enhanced heat transport by latent heat through vaporization and subsequent condensation [*Cass et al.*, 1984] were also not considered. Although we expect that temperature effects are minor for the experimental temperature regimes presented herein, subsequent studies will fully account for the temperature influence on flow and transport.

[19] Several small modifications of HYDRUS-2D were implemented to make numerical heat transport experiments possible. The public version of HYDRUS-2D can handle either Dirichlet (temperature) or Cauchy (heat flux) boundary conditions, but it has no provisions for a heat source without a corresponding water flux. The heat pulse probe boundary condition was implemented by adding a zero-order source term to (5), which was active only for the nodes representing the heat pulse probe during heat pulse application. In simulations for which a single node represented the heat pulse probe (case P), the corresponding heat flux at this single node was 57.7 W m^{-1}. When simulating the finite heat source experiments (case F), several nodes were used to describe the geometry of the heat pulse probe, with the heat source strength distributed uniformly across these nodes.

2.6. Numerical Experiments

[20] Corresponding to objectives 1 through 3, we present three numerical heat transport experiments (experiments I, II, and III). The first experiment (I) analyzes the influence of the finite probe geometry of the heater probe on the optimized soil thermal and water flux density values. To achieve this, we compare optimization results with a line heater needle of infinitely small diameter (case P) with those using a finite size 1-mm-diameter heater probe (case F). In the second experiment (II) we compare results of inverse modeling simulations with and without the dispersion term in (7). We show results for both unsaturated and saturated flow conditions and for a range in water flux density (q_w) and thermal dispersivity (β) values. We show the contribution of the dispersive component to be a function of the KJJ and Pe numbers, with increasing significance as the water flux density becomes larger. Finally, in the third experiment (III) we demonstrate how the functional dependence of the soil thermal properties with water content and

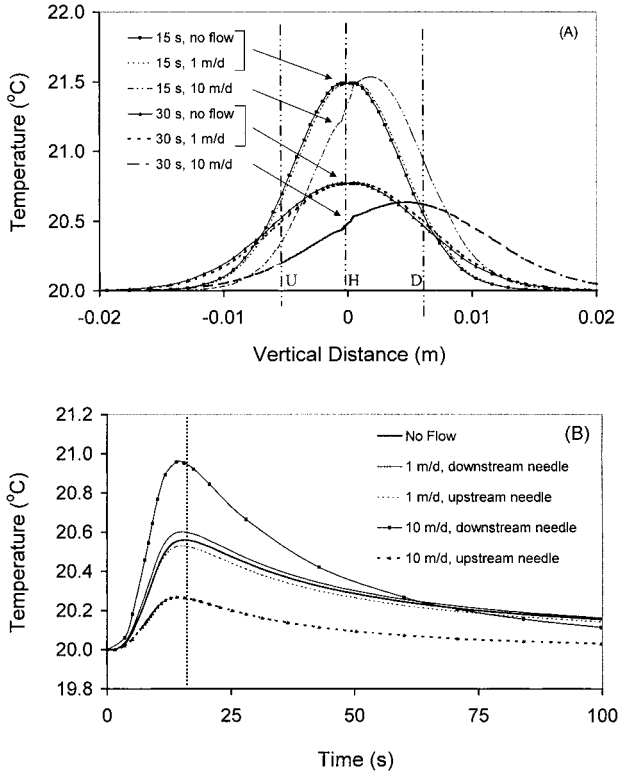

Figure 4. (a) Simulated spatial temperature distributions, 15 and 30 s after heating, for q_w values of 0, 1, and 10 m d^{-1} (b) Simulated temporal distributions at the upstream (U) and downstream (D) temperature sensors for q_w values of 0, 1, and 10 m d^{-1} (no thermal dispersion).

pore water velocity can be estimated from a single experiment, using inverse modeling. The outcome of this experiment will show that the functional dependence of bulk soil thermal conductivity and bulk soil heat capacity with water content can be estimated using IM.

[21] Parameter optimizations were carried out with a single set of initial estimates, in which we evaluated effects of needle geometry (experiment I) and thermal dispersion (experiment II) on parameter estimation of thermal and water flow properties. Although, in general, we recommend using various combinations of different initial estimates, a single optimization was justified because of the relative closeness of the initial parameter values to their true values. Multiple sets of initial parameter estimates were used in experiment III, with optimization results reported only for the smallest value of the objective function. The initial estimate for q_w was twice its true value; initial estiamtes for θ were 0.33 and 0.28 m^3 m^{-3} for the saturated and unsaturated problems, respectively, whereas the initial value of λ_0 was set to 2.5 W m^{-1} K^{-1}. For cases with variable β_L its initial value was set to twice its true value as was done for the flux density estimate.

3. Results and Discussion

3.1. Analysis of Convective Heat Transport

[22] To improve our intuitive understanding of the contribution of diffusive and convective heat transport during HPP measurements, we show in Figure 4a the spatial temperature distribution around the heater (H) for two simulation times, following a typical 8-s heating period (57.7 W m^{-1}) at location H. For illustrative purposes the origin is defined at the heater location, and the spatial coordinate is along the z direction only. For this example the soil is saturated (θ_s = 0.31 m^3 m^{-3}), and temperature distributions are presented for water flux density (q_w) values of 0.0 (no flow), 1.0, and 10.0 m d^{-1}. The finite dimensions of the heater source (1 mm) were accounted for in the flow calculations. In addition, Figure 4b shows the corresponding temperature values as a function of time at both the downstream (D) and upstream (U) thermocouple locations. Note that for both flow velocities used here, the KJJ number is equal to zero since dispersion was not considered.

[23] Focusing on the case without heat convection first (no flow), the symmetrical temperature distribution around the heater location in Figure 4a clearly shows the dissipation of the temperature signal around the heater. Heat transport is by conduction only, causing identical pulse-type temperature signals at thermocouple locations D and U (no flow (Figure 4b)). When including convection, the temperature signal generated at position H will move in the direction of D with a convective heat pulse velocity V_h of $\sim$15.95 m d^{-1}, as calculated from (11) for a q_w value of 10 m d^{-1} (or averagepore water velocity V_w of 32.3 m d^{-1}). This will move the heat pulse $\sim$0.0055 m after 30 s. As is evident by visual inspection of Figure 4a, the temperature signals for the case with q_w = 1.0 m d^{-1} is about equal to the no-flow case. Hence it is expected that accurate water flow velocity measurements with the HPP are unlikely for these or lower water flow velocities. Clearly, the sensitivity of the water flux density measurements will depend on the temperature measurement accuracy, but as *Ren et al.* [2000] concluded, the lower detection limit of water velocity is $\sim$0.06 m d^{-1} for a thermocouple measurement accuracy of 0.01 K. For steady state water flow, with uniform water content distribution along its pathway, the shape of the temperature signal should be approximately independent of flow rate but translated over a distance determined by the convective heat pulse velocity V_h. Inspection of the temperature signal as a function of time (Figure 4b) also shows that the downstream peak temperatures will increase with increasing water flow velocities. This is caused by the slightly smaller travel time of the faster heat pulse (note differences in t_{max} between water flow velocities, as determined from its position relative to the dotted vertical line), thereby reducing lateral heat loss by conduction. As is expected, the temperature peak of the downstream thermocouple is always higher than for the upstream location, with the difference between thermocouple locations increasing as the flow velocity increases. The results of Figure 4 also clearly illustrate that incorrect thermal property estimations with HPP measurements are obtained for water fluxes >1.0 m d^{-1}, unless the water flux is taken into consideration.

[24] Figure 5 shows the effect of dispersivity on the temperature signal at the upstream and downstream needle, using a q_w value of 1 m d^{-1}. To document the heat movement in the transverse direction, we also included an additional measurement point 6 mm away from the heat source in the horizontal direction, i.e., perpendicular to the direction of water flow (transverse thermocouple T (Figure 2). As is obvious from (5) and (7), dispersion has an effect similar to thermal conduction on the temperature distribution. However, while thermal conduction acts symmetrically in all directions, dispersion manifests itself preferentially in the direction of water flow (since it is usually assumed that β_T = $0.1\beta_L$). For the case with no flow the temperature profile will be

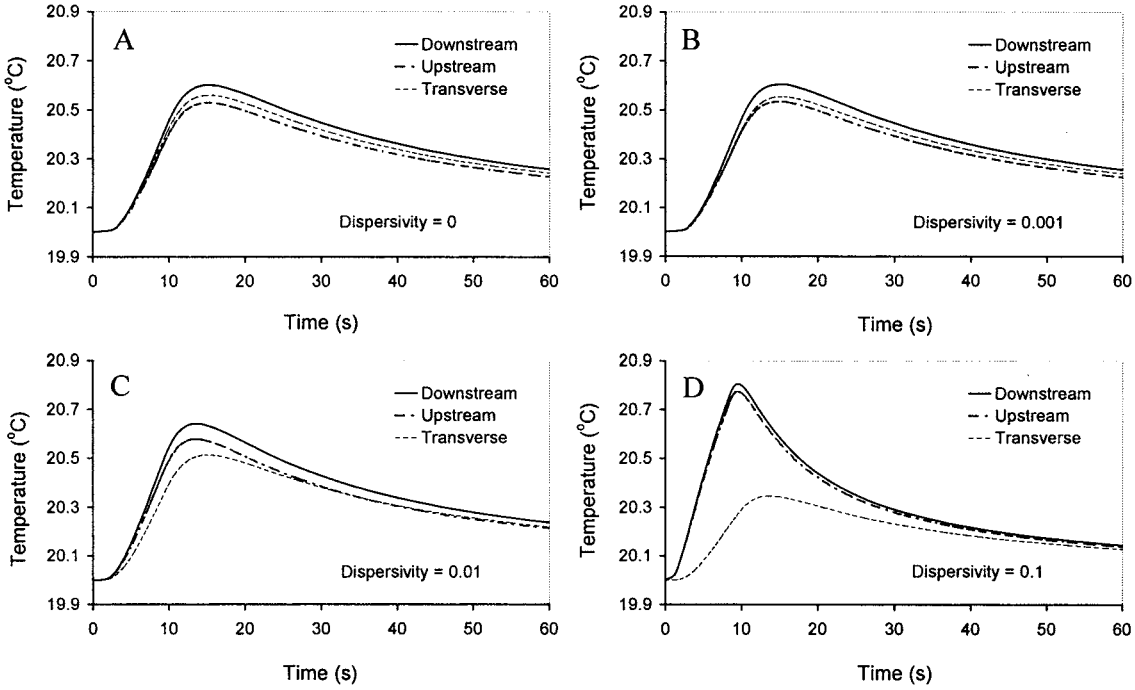

Figure 5. Temperature as a function of time for upstream, downstream, and transverse thermocouple locations for dispersivity values of (a) 0.0, (b) 0.001, (c) 0.01, and (d) 0.1 m (q_w = 1.0 m d^{-1}).

identical for all three measurement positions, as demonstrated in Figure 4a.

[25] Water flow (without dispersion) results in an asymmetrical temperature profile, with a larger temperature peak at the downstream location than at the upstream location and with the transverse thermocouple recording intermediate temperatures (Figure 5a). Larger dispersivities will cause higher temperature peaks (ΔT_{max}) and earlier arrival of the temperature front (t_{max} decreases) at both downstream and upstream locations because of the increased effective thermal conductivity (Figures 5b through 5d). As the effective conduction (including the dispersion contribution) becomes dominant over convection (smaller *Pe* numbers), the temperature difference at the peak between the upstream and downstream tends to disappear (Figure 5d), thereby reducing the flux information. This result is in agreement with *Ren et al.* [2000], who found increasing discrepancies between measured and predicted temperature fields for increasing flux densities within their range of water flux densities between 2 and 6 $\times$ 10^{-5} m s^{-1} (1.73–5.18 m d^{-1}). Table 2 summarizes numerically results presented in Figure 5 as obtained with different values of dispersivity for the same water flux of 1 m d^{-1}. Note that the results span conditions for heat transport dominated by conduction (KJJ values between 0 and 0.022) to conditions where the dispersion component is about twice as large as conduction (KJJ = 2.2). We find that while increasing the dispersivity (at this water flux of 1 m d^{-1}) from zero to 0.1 m, the corresponding temperature difference (ΔT_{max}) between the upstream and downstream locations decreases by more than a half. Consequently, using the predicted temperature difference (ΔT_{max}) assuming zero dispersion will underestimate the water flux density [see *Ren et al.*, 2000, Figure 9], increasingly more so for soils with larger dispersivities or with increasing water velocities.

[26] As dispersion acts preferentially in the direction of water flow, less heat is available for conduction in the lateral flow directions (perpendicular to water flow), thereby significantly reducing the peak temperature at the transverse thermocouple location (T). For a dispersivity of only 0.01 m the peak temperature at the transverse location is already smaller than at the upstream location (Figure 5c). Thus dispersion causes differences in temperature between longitudinal (upstream and downstream thermocouple locations) and transverse locations (transverse thermocouple

Table 2. Influence of Longitudinal Dispersivity β_L on Maximum Temperatures at the Downstream (T_D), Upstream (T_U), and Transverse (T_T) Locations at Time t_{max} on the Temperature Difference (ΔT_{max}) Between the Upstream and Downstream Locations at Time t_{max} and on the KJJ Number

β_L, m	t_{max},[a] s	T_D, °C	T_U, °C	T_T, °C	ΔT_{max}, °C	KJJ,[b] dimensionless
0	15.135	20.601	20.529	20.560	0.072	0
0.001	15.135	20.606	20.535	20.555	0.071	0.022
0.01	13.666	20.641	20.578	20.508	0.063	0.22
0.05	10.670	20.747	20.703	20.355	0.044	1.1
0.10	9.452	20.806	20.775	20.271	0.031	2.2

[a] Here t_{max} is time of the maximum temperature at downstream location.
[b] Here q_w = 1 m d^{-1}.

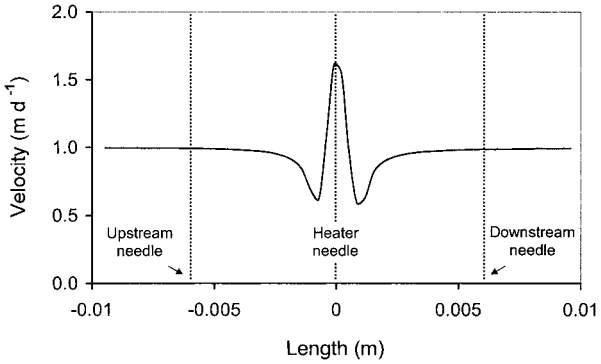

Figure 6. Water flux density distribution along transect AA′ of Figure 2.

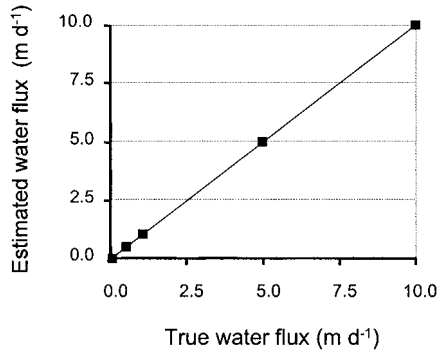

Figure 7. Comparison of estimated with "true" flux density values for the case with no thermal dispersion (experiment I).

needle). We therefore suggest that inclusion of a third transverse thermocouple needle in the heat pulse sensor (see Figure 2) is needed to extend the range of accurate water velocity measurements to higher flow velocities.

3.2. Experiment I: Effect of Needle Geometry on IM of Thermal and Water Flow Properties

[27] We assume no significant influence of the geometry of the temperature needle of the HPP on temperature measurements, as we expect that the thermocouple will sense an integrated value around the sensor needle. We thus assume that the higher temperature arriving at the upstream end of the temperature needle due to heat pulse will be balanced by the lower temperature at the downstream end of the needle. The finite geometry of the heater probe can, however, affect the temperature response of the sensor probe in two ways. First, for conditions of unidirectional water flow in the z direction the physical presence of the heater probe will distort the flow field of water around the heater needle, thereby affecting the convective heat transport component in (5). Simulation results, indeed, showed the presence of such flow distortion. Specifically, water flow converged in the x direction around the heater needle to cause increased local flow velocities but diverged near the top and bottom of the heater needle, leading to reduced water flow velocities in these regions. An example of the vertical distribution of water flow rate (q_w) for saturated conditions (q_w = 1 m d^{-1}) as calculated numerically across the AA′ section (Figure 2) is given in Figure 6. Velocities decreased as the moving water approached the top of the needle but increased as water moved around the needle and then decreased again immediately below the needle. The maximum water velocity was ~3 times larger than the minimum velocity (Figure 6).

[28] A second effect may be caused by the decreased distance for the heat pulse to move before arriving at the downstream sensor needle. Specifically, for a needle diameter of 1.0 mm and a center-to-center distance (r) between the heater and downstream needles of 6.0 mm the finite diameter of the heater needle reduces the total travel distance of the heat front from 6.0 to 5.5 mm, or ~8%, as compared to a 6-mm travel distance assuming that the heater needle is inifinitely thin.

[29] In order to evaluate these two effects of needle geometry on estimation of thermal and water flow properties we carried out a numerical study, in which we considered the two following cases. In the first case we simplified the problem by assuming a point heater source (case P), thus neglecting effects of geometry, i.e.,

Table 3. Influence of Probe Geometry on Parameter Optimization Results With No Dispersion[a]

Case	True Values			Pe[b]	Optimized Values			Error[c]		
	q_w, m d^{-1}	θ, dimensionless	λ_0, W m^{-1} K^{-1}		q_w, m d^{-1}	θ, dimensionless	λ_0, W m^{-1} K^{-1}	q_w, %	θ, %	λ_0, %
P						0.2996	2.286	...	−3.4	3.2
F	0	0.310	2.215	0		0.310	2.215	...	0.0	0.0
P						0.1474	1.845	...	−4.9	3.2
F	0	0.155	1.788	0		0.155	1.778	...	0.0	−0.6
P					0.0989	0.3035	2.308	−1.1	−2.1	4.2
F	0.1	0.310	2.215	0.0008	0.0973	0.310	2.217	−2.7	0.0	0.1
P					0.5005	0.2999	2.287	0.1	−3.3	3.3
F	0.5	0.310	2.215	0.004	0.497	0.309	2.210	−0.6	0.3	−0.2
P					1.016	0.3036	2.307	1.6	−2.1	4.2
F	1.0	0.310	2.215	0.008	0.994	0.311	2.195	−0.6	0.3	−0.9
P					1.013	0.1495	1.857	0.3	−3.5	3.9
F	1.0	0.155	1.788	0.01	1.001	0.1548	1.787	0.0	0.0	0.0
P					5.031	0.3031	2.294	0.6	−2.2	3.6
F	5.0	0.310	2.215	0.04	4.994	0.308	2.216	−0.1	0.6	0.0
P					9.995	0.3029	2.279	−0.1	−2.3	2.9
F	10.0	0.310	2.215	0.079	9.997	0.310	2.216	0.0	0.0	0.0

[a] P represents the point case; F represents the finite case. No dispersion is $\beta_L = 0$.
[b] C_w = 48.38 W d m^{-3} K^{-1}, and d = 0.00036 m.
[c] Error = $[(y_{opt} - y_{true})/y_{true}]100\%$, $y = q_w$, θ, or λ_0.

Table 4a. Influence of Dispersion on Parameter Optimization Results Using Information From the Upstream and Downstream Locations

Case	Pe[a]	True Values					KJJ, dimensionless	Optimized Values					Errors[b]				
		q_w, m d^{-1}	θ, dimensionless	β_L, m	λ_0, W m^{-1} K^{-1}	λ_{eff}, W m^{-1} K^{-1}		q_w, m d^{-1}	θ, dimensionless	λ_0, W m^{-1} K^{-1}	λ_{eff}, W m^{-1} K^{-1}	β_L, m	q_w, %	θ, %	λ_0, %	λ_{eff}, %	β_L, %
1a[c]	0.0077	1.0	0.310	0.001	2.215	2.26	0.022	0.989	0.304		2.24		−1.1	−1.9		−0.9	
1b								1.042	0.334	2.13		0.0044	4.2	7.7	−3.8		340
1c									0.310	2.212		0.00105		0.0	−0.1		5.0
2a	0.0064	1.0	0.310	0.01	2.215	2.70	0.22	0.904	0.259		2.46		−9.6	−16.5		−8.9	
2b								1.037	0.338	2.17		0.013	3.7	9.0	−2.0		3.0
2c									0.315	2.196		0.0100		1.6	1.1		−0.8
3a	0.0038	1.0	0.310	0.05	2.215	4.63	1.1	0.720	0.144		3.35		−28.0	−53.5		27.6	
3b								1.133	0.388	2.18		0.056	13.3	25.2	−1.6		12.0
3c									0.309	2.220		0.0497		−0.3	0.2		−0.6
4a	0.0025	1.0	0.310	0.10	2.215	7.05	2.2	0.602	0.076		4.33		−39.8	−75.5		−38.6	
4b								1.151	0.400	2.36		0.10	15.1	29.0	6.5		0.0
4c									0.313	2.196		0.1012		1.0	1.1		1.2
5a	0.064	10.0	0.310	0.001	2.215	2.70	0.22	9.135	0.259		2.46		−8.6	−16.5		−8.9	
5b								13.57	0.384	2.31		0.0021	35.7	23.9			110.0
5c									0.310	2.212		0.001010		0.0	−0.1		1.0
6a	0.025	10.0	0.310	0.01	2.215	7.05	2.2	10.38	0.0012		6.87		3.9	−99.6		−2.5	
6b								13.33	0.511	2.04		0.011	33.3	41.1	−7.9		10.0
6c									0.310	2.215		0.01001		0.0	0.0		0.1
7a	0.0095	1.0	0.155	0.001	1.788	1.83	0.027	0.884	0.103		2.01		−11.6	−33.5		9.8	
7b								0.994	0.152	1.80		0.0096	−0.6	−1.9	0.6		−4.0
7c									0.156	1.784		0.0011		0.6	−0.2		10.0
8a	0.0077	1.0	0.155	0.01	1.788	2.27	0.27	0.984	0.149		1.81		−1.6	−3.9		−20.3	
8b								1.156	0.225	1.56		0.012	15.6	45.2	−12.8		20.0
8c									0.155	1.786		0.0101		0.0	−0.1		0.1
9a	0.0026	1.0	0.155	0.1	1.788	6.62	2.7	1.192	0.0002		5.36		19.2	−99.9		−19.0	
9b								0.973	0.144	1.84		0.097	2.7	−7.1	2.9		3.0
9c									0.153	1.797		0.099		−1.3	0.5		1.1

[a] C_w = 48.38 W d m^{-3} K^{-1}, and d = 0.00036 m.
[b] Error = $[(y_{opt} - y_{true})/y_{true}]100\%$.
[c] For case a, assume $\beta_L = 0$; optimize q_w, θ, and $\lambda_{eff}(=\lambda_0)$. For case b, optimize β_L, q_w, θ, and λ_0. For case c, fix q_w to its "true" value; optimize β_L, θ, and λ_0.

Table 4b. Influence of Dispersion on Parameter Optimization Results Using Temperature Information From the Transverse Location in Addition to Upstream and Downstream Locations

Case	Pe[a]	True Values					KJJ, dimensionless	Optimized Values				Errors[b]			
		q_w, m d^{-1}	θ, dimensionless	β_L, m	λ_0, W m^{-1} K^{-1}	λ_{eff}, W m^{-1} K^{-1}		q_w, m d^{-1}	θ, dimensionless	λ_0, W m^{-1} K^{-1}	β_L, m	q_w, %	θ, %	λ_0, %	β_L, %
1d[c]	0.0077	1.0	0.310	0.001	2.215	2.26	0.022		0.310	2.213	0.00102		0.0	−0.1	2.0
1e								0.999	0.310	2.215	0.000991	−0.1	0.0	0.0	−0.9
2d	0.0064	1.0	0.310	0.01	2.215	2.70	0.22		0.311	2.224	0.0104		0.3	0.4	4.0
2e								0.999	0.310	2.215	0.0100	−0.1	0.0	0.0	0.0
3d	0.0077	1.0	0.310	0.05	2.215	4.63	1.1		0.310	2.213	0.0498		0.0	−0.1	−0.4
3e								1.000	0.310	2.215	0.0500	0.0	0.0	0.0	0.0
4d	0.0038	1.0	0.310	0.10	2.215	7.05	2.2		0.310	2.215	0.1008		0.0	0.0	0.8
4e								0.998	0.310	2.216	0.1002	−0.2	0.0	0.0	0.2
5d	0.064	10.0	0.310	0.001	2.215	2.70	0.22		0.310	2.215	0.001004		0.0	0.0	0.4
5e								9.994	0.310	2.214	0.000999	0.0	0.0	0.0	−0.1
6d	0.038	10.0	0.310	0.01	2.215	7.05	2.2		0.310	2.216	0.1000		0.0	0.0	0.0
6e								9.996	0.310	2.216	0.01000	0.0	0.0	0.0	0.0
7d	0.0095	1.0	0.155	0.001	1.788	1.83	0.027		0.155	1.788	0.0010		0.0	0.0	0.0
7e								0.999	0.155	1.788	0.0010	0.1	0.0	0.0	0.0
8d	0.0077	1.0	0.155	0.01	1.788	2.27	0.27		0.155	1.788	0.0100		0.0	0.0	0.0
8e								0.998	0.155	1.787	0.0100	−0.2	0.0	0.0	0.0
9d	0.0026	1.0	0.155	0.1	1.788	6.62	2.7		0.155	1.788	0.100		0.0	0.0	0.0
9e								0.999	0.155	1.788	0.100	0.1	0.0	0.0	0.0

[a] C_w = 48.38 W d m^{-3} K^{-1}, and L = 0.00036 m.
[b] Error = $[(y_{opt} - y_{true})/y_{true}]100\%$.
[c] For case d, fix q_w to its "true" value; optimize β_L, θ, and λ_0. For case e, optimize β_L, q_w, θ, and λ_0.

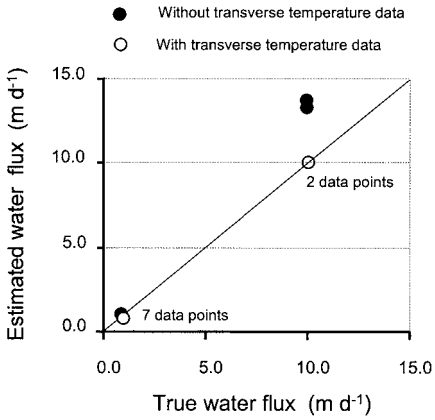

Figure 8. Comparison of estimated with "true" flux density values without (solid circles) and with (open circles) inclusion of the transverse (T) temperature data in the objective function (experiment II).

flow distortion and decreased distance between probes. In the second case, by considering a finite geometry source (case F) we took geometry effects fully into account. The sensitivity analysis involved the following procedural steps. First, a forward simulation was conducted with the HYDRUS-2D code, with specific values for θ, steady state vertical water flux density (q_w), a finite geometry source, and the hydraulic and thermal properties of Table 1. The resulting simulated $T(z,t)$ data for both the upstream and downstream thermocouple sensor (case F) were assumed to be the "true" temperature values (as measured with the 1.0-mm-diameter heater needle). In the subsequent inverse modeling (IM) step these true data were used in the objective functions as the measured values, whereas θ, q_w, and λ_{eff} were optimized for both the point (P) and finite (F) case. The simulation results are given in Table 3. The estimation of these three parameters allows direct computation of the thermal diffusivity (κ) and convective heat pulse velocity (V_h), provided the bulk volumetric heat capacity (C_{bulk}) is known. Hence it is assumed that bulk soil density (ρ_b) and soil specific heat (c_s) values are available. For mineral soils (contribution of organic matter content to bulk soil heat capacity can be ignored) the c_s is usually between 0.7 and 0.9 J kg^{-1} K^{-1} and varies with mineral type and quartz content [*de Vries*, 1963]. Although ignored, there is also some temperature dependence on c_s [*Kay and Goit*, 1975; *Hopmans and Dane*, 1986a].

[30] The geometry effect may be considered negligible if the optimized heat and flow parameters are equal to their true values. The error in the last three columns of Table 3 is expressed relative to the true value. When considering all results combined, ignoring the effects of the true geometry of the heat source on heat transport resulted in a slight underestimation of the water content values by ~3% and an overestimation of the thermal conductivities by ~3–4%. For no-flow conditions the error analysis by *Kluitenberg et al.* [1995] concluded that errors in the thermal properties were <1% using a ratio of heater radius to sensor needle spacing of 0.08 and a heating time of 8 s. Therefore we tentatively conclude that the convective heat transport component increases the uncertainty of the soil thermal parameters. However, if the finite probe geometry is included in the heat transport simulations, we conclude that predictions of water flux density, water content, and thermal conductivity are excellent, with estimation errors <1% for q_w > 0.5 m d^{-1}. Moreover, even though the water flux estimation error is close to 3% for the smallest water velocity (q_w = 0.1 m d^{-1}), the prediction errors of water content and thermal conductivity are practically zero. We must note that the finite probe geometry simulations assumed that all HPP needles have an infinitely small heat capacity and large thermal conductivity, so that the "true" temperature distribution is not affected by the thermal properties of the HPP. The real thermal properties of the high-conductive epoxy within the needles though are about equal to those of a wet soil, implicating that future modeling studies should more accurately represent the thermal properties of the HPP. The estimated q_w values are compared with the corresponding true values in Figure 7. We note that the optimized values in Table 3 were obtained for both unsaturated and saturated soil conditions with water flux density values ranging between 0.1 and 10.0 m d^{-1}, while assuming zero thermal dispersion.

[31] Taking into account the physical size of the heater needle is also important for optimizing experimental conditions. For example, heat pulse strength must be controlled so that maximum soil temperatures will not enhance water flow as may occur by vapor transport. For equal source strengths, because of its larger surface area, the finite heat source will cause a smaller increase in local soil temperature than the point source. For example, on the basis of numerical simulations, maximum soil temperature at the source-soil interface for the 57.7 W m^{-1} heat pulse reached ~35°C for the point source, while it was ~29°C near the finite source (1-mm diameter). Hence one can safely use larger energy sources, thereby improving the resolution at the sensor needle, when using larger heater needles. For example, if the temperature range during the

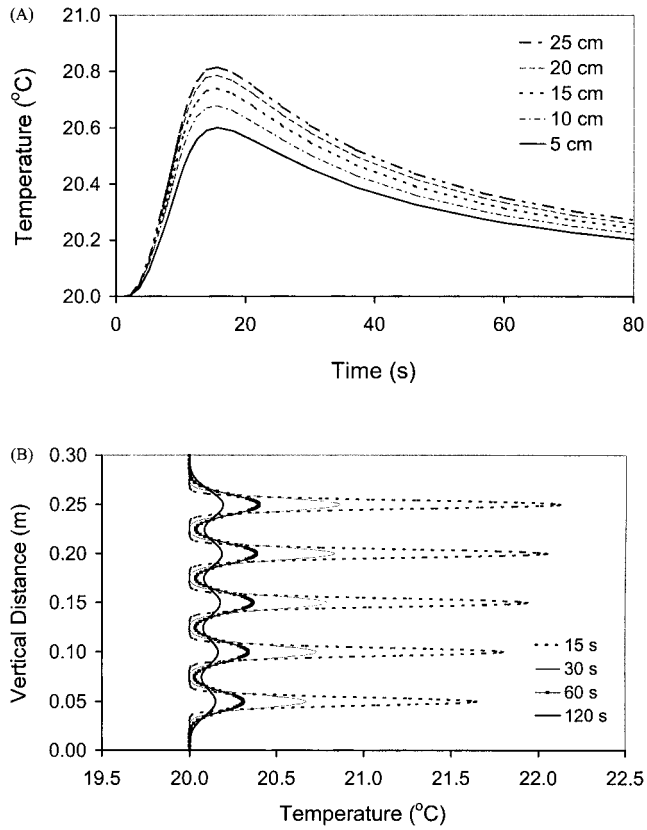

Figure 9. (a) Temperatures measured with heat pulse probes at five locations within the soil column and (b) temperatures along the z axis at four different times for experiment III.

Table 5. Estimation of Thermal Properties Using Inverse Modeling of a Simulated Column Experiment[a]

Case	Position z, m	True Values			Estimated					
		θ, dimensionless	λ_0, W m^{-1} K^{-1}	C_s, J m^{-3} K^{-1}	θ, dimensionless	λ_0, W m^{-1} K^{-1}	C_s, J m^{-3} K^{-1}	b_0, W m^{-1} K^{-1}	b_1	b_2
a	0.25	0.105	1.544		0.110	1.550				
					(0.0001)	(0.001)				
	0.20	0.123	1.651		0.128	1.617				
					(0.0006)	(0.0044)				
	0.15	0.150	1.766		0.160	1.720				
					(0.0007)	(0.0051)				
	0.10	0.193	1.919		0.196	1.886				
					(0.0002)	(0.0018)				
	0.05	0.260	2.105		0.265	2.056				
					(0.0007)	(0.0047)				
b								0.332	−1.628	4.195
								0.230	−2.395	4.900
								(0.0089)	(0.0533)	(0.0443)
c				1.920×10^6			1.920×10^6	0.237	−2.354	4.865
							(242.2)	(0.0082)	(0.0489)	(0.0406)

[a] The 95% confidence intervals are indicated within parentheses. (True values of $b_0 = 0.228$, of $b_1 = -2.406$, and $b_2 = 4.909$).

experiment must be below 35°C, a stronger source than 57.7 W m^{-1} can be used when considering the actual dimension of the heater needle.

3.3. Experiment II: Effect of Thermal Dispersion on Parameter Estimation of Thermal and Water Flow Properties

[32] To investigate the influence of thermal dispersion on soil heat transport and on indirectly estimated heat transport and water flow parameters, forward simulations were conducted for a range of water flux density, water content, and dispersivity values, as indicated by the true values in Tables 4a and 4b. Cases 1, 2, and 4 from Tables 4a and 4b, as well as the case with zero dispersion, are shown in Figure 5. Initial estimates of optimized parameters were selected as in experiment I. We note that the dispersion contribution to the total effective thermal conductivity increases as the flux density (q_w) and dispersivity (β_L) increase and the water content (θ) decreases. The increasing dispersion effect is described by increasing values of the KJJ number. In the second IM step the resulting temperatures at the upstream and downstream locations were used as input to the inverse model, from which the water flux q_w, the water content θ, and either the effective thermal conductivity λ_{eff} (zero thermal dispersion (case a)) or the bulk soil thermal conductivity λ_0 and the thermal dispersivity β_L (case b) were estimated.

[33] It is rather difficult to interpret the optimization results when information from only the upstream and donwstream locations is used. In case a, optimization results tend to underestimate water fluxes and significantly underestimate water contents and effective thermal conductivities with increasing true dispersivity. If thermal dispersion is neglected (case a), the bulk soil thermal conductivity is increasingly overestimated with increasing dispersivity. Optimization results tend to slightly improve when λ_0 and β_L are estimated simultaneously (case b). When dispersion is included in the inverse analysis, dispersivity is estimated with a reasonable precision, but the water fluxes, as well as the water contents, tend to be overestimated. Temperature signatures at the upstream and downstream locations apparently do not contain enough information for successful simultaneous optimization of these two sets of parameters, i.e., either q_w, θ, and λ_{eff} in case a or q_w, θ, λ_0, and β_L in case b.

[34] The difficulty of the simultaneous estimation of flux q_w and dispersivity β_L stems from the fact that these two processes tend to have opposite effects on the difference in temperatures at the upstream and downstream locations. Increasing flux tends to increase this temperature difference, while increasing dispersivity tends to decrease it. At the same time, increasing dispersion has the same effect as increasing heat conductivity on the arrival of the temperature peak at these two locations. Optimization results improve significantly when water flux q_w is known. In this case (case c) the water content θ, the bulk soil thermal conductivity λ_0, and the heat dispersivity β_L were estimated with reasonable precision.

[35] As hypothesized above, valuable information about flux and dispersivity can be collected when temperature measurements at the upstream and downstream locations are complemented with temperature measurements at the transverse location of the heater needle. This is demonstrated in Table 4b where temperatures measured at three locations (upstream, downstream, and transverse) were used to estimate simultaneously θ, λ_0, and β_L for case d or additionally q_w for case e. In either case, λ_{eff} values are determined from optimized β_L and q_w values using (7) with a known C_w value. Inspection of the results in Table 4b reveals that both parameter sets were successfully back calculated using inverse analysis with zero estimation errors for all but one case. A comparison of estimated with true water flux density values for cases c (without transverse temperature measurememts) and e (with

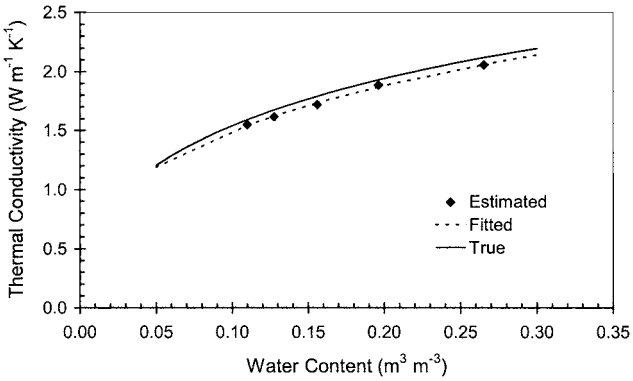

Figure 10. True and fitted thermal conductivity functions for the column experiment III. Thermal conductivity function was fitted to the estimated data values of case a.

transverse temperature measurements) is presented in Figure 8. We note that the number of displayed data points is nine (see Table 4b) for each case, however, most of these coalesce because of nearly identical values. These results suggest that information from all three sensor needles can be used advantageously in estimating simultaneously the water flux and the thermal dispersivity, especially at the higher water fluxes.

3.4. Experiment III: Parameter Optimization of Thermal Properties

[36] To demonstrate the application of IM for estimation of the functional dependence of the soil thermal properties with water content, a numerical column experiment was conducted. We suggest that a similar laboratory experiment may be used for estimating a soil's thermal properties, as determined by its thermal conductivity and bulk soil heat capacity.

[37] The simulated soil column was 30 cm long, with water being in static hydraulic equilibrium with the water table located at the base of the column. Hence the soil water matric potential was zero at the base of the column and linearly decreased to -30 cm at the soil surface. A no-flow condition was selected since it can be achieved relatively easily in a laboratory. However, we suggest that the same experimental setup can be used for steady state flow, allowing simultaneous estimation of soil thermal and hydraulic function parameters. Soil hydraulic and thermal properties used in this experiment are identical to those used in the previous experiments and are summarized in Table 1. Although the matric head range for this experiment may appear small, the corresponding water content range for the Tottori sand (see Figure 3a) was between 0.31 (base of column) and $\sim$0.11 (top of column). The temperature responses of five vertically placed heat pulse probes were simulated at 5, 10, 15, 20, and 25 cm below the soil surface. Using the vertical HPP arrangement, the central heater needle was placed at the exact depth, whereas the two sensor needles where either above or below the heater. An 8-s heat pulse of 57.7 W m^{-1} was applied to each probe, and temperature responses were recorded at the sensor needles during a subsequent 120-s monitoring period. The temperature information was used in the inverse analysis by including $T(z,t)$ data in the objective function of (13). Because water content values differed between probe locations (from 0.105 to 0.260 m^3 m^{-3}), the temperature signatures were different for each depth (Figure 9), with increasing temperature amplitudes for the near-surface sensors because of the corresponding decrease in soil water and hence bulk soil heat capacity.

[38] We conducted two inverse modeling analyses with the simulated temperature data (Table 5). First, the temperature signatures of each HPP were analyzed separately (case a), from which water content and thermal conductivity data were estimated for each location. The resulting soil water retention (matric potential is known since the flow experiment is in hydraulic equilibrium) and thermal conductivity data can be directly used to fit soil water retention and thermal conductivity function parameters. Results of the optimized thermal conductivity data are presented in Table 5 and in Figure 10 (diamonds and dashed line). We note that water content values were slightly overestimated, leading to a small underestimation ($\sim$2%) of thermal conductivity across the experimental water content range. This small estimation error was likely caused by the underlying assumption that each HPP measurement represented uniform water content for the soil between the HPP needles. However, because of the vertical arrangement of the HPPs in a soil column that is in hydraulic equilibrium with the water table, the soil water content between the heater and downstream sensor needles must increase downward. Vertical placement of the heat probe was chosen, since it allows simultaneous estimation of vertical flux density, either downward (infiltration) or upward (evaporation). Hence we would expect an even more accurate estimation of the thermal conductivity function if the HPP were installed horizontally. The IM method used does not allow for the simultaneous estimation of the bulk soil heat capacity and the water content, since these two variables are fully correlated by the thermal diffusivity term in (9).

[39] In the second estimation procedure (cases b and c) the temperature signatures at all five locations were analyzed simultaneously so that parameters of the thermal conductivity function were estimated directly, with (case b) or without (case c) additional estimation of the bulk soil heat capacity of the solid phase (C_s). Simultaneous estimation of both soil thermal properties is now possible, since the water content is assumed to be known a priori from the soil water retention curve. In both cases the estimated thermal conductivity function parameters were practically identical to their true values, and the function coincides with the true function in Figure 10 (solid line). Also, the heat capacity of the mineral phase could be estimated accurately, once the water content was known.

[40] In summary, this third experiment (III) has shown that the functional dependence of the bulk soil thermal conductivity and bulk soil heat capacity with water content can be estimated from a simple laboratory experiment when integrated with inverse modeling. Moreover, if the bulk soil heat capacity is known, the suggested experimental setup allows simultaneous estimation of soil water retention (when combined with matric potential measurements) and unsaturated hydraulic conductivity (through water flux estimation) parameters.

4. Summary and Conclusions

[41] Traditional data analysis of the heat pulse probe is based on the analytical solution of the heat transport equation in a uniform static or steady state water flow field. Although such analysis proved to be a powerful tool in estimating soil thermal properties, some of the underlying assumptions may not be valid in typical laboratory and/or field situations. In this study, we used a numerical solution of the heat transport equation to evaluate the effects of the physical size of the heater needle on the water flow field and the temperature response for a range of water flux densities. We conclude that error estimates of water flux and soil thermal properties can be reduced from $\sim$3% to near zero if the physical

size of the heater needle is included in the numerical solution of the heat transport equation.

[42] The influence of thermal dispersion on heat transport and estimated thermal properties and water flow densities was analyzed using parameter estimation by inverse modeling. On the basis of our analyses we suggested an explanation for increasing discrepancies between measured and predicted temperature fields for increasing flux densities as reported by *Ren et al.* [2000]. Since increasing flux tends to increase the difference in temperatures between the upstream and downstream measurement locations, while increasing dispersivity causes decreasing temperature differences, the flux density cannot be accurately estimated without considering dispersive heat flux. Thus we conclude that flux density can be estimated only when thermal dispersivity is known and vice versa. Since the analytical solution of *Ren et al.* [2000] did not take thermal dispersion into account, their predicted water fluxes were significantly underestimated. Although it is intuitively expected that solute and thermal dispersivity values should be similar, few if any studies have been conducted to determine thermal dispersivity in unsaturated soils.

[43] To avoid the need for prior knowledge of dispersivity, we suggest using an additional sensor located in the transverse direction of the line heat source. From an additional sensitivity analysis we evaluated the feasibility of such an approach for the estimation of thermal properties and water flow densities using inverse modeling. We showed that temperatures collected at three sensors (two parallel and one perpendicular to water flow) could provide the required information for simultaneous and accurate estimation of water flux, heat dispersivity, and soil thermal properties. If heat dispersivity values are of similar magnitude as the dispersivity defined for solute transport (as suggested by *De Marsily* [1986]), the inverse modeling method presented herein may be a valuable tool for estimation of solute transport dispersivity. Further experimental evidence, however, is needed to support this conclusion.

[44] Finally, we demonstrated the general application of inverse modeling to estimate the soil thermal properties and their functional dependence on volumetric water content. In a subsequent study we will present additional results, regarding the potential application of inverse modeling to estimate solute transport properties in addition to the thermal and flow properties when combined with multineedle heat pulse probe measurements.

References

Bear, J., *Dynamics of Fluids in Porous Media*, Dover, Mineola, New York, 1972.

Bristow, K. L., Measurement of thermal properties and water content of unsaturated sandy soil using dual-probe heat-pulse probes, *Agric. For. Meteorol.*, *89*, 75–84, 1998.

Bristow, K. L., G. S. Campbell, and C. Calissendorff, Test of a heat-pulse probe for measuring changes in soil water content, *Soil Sci. Soc. Am. J.*, *57*, 930–934, 1993.

Bristow, K. L., G. J. Kluitenberg, and R. Horton, Measurement of soil thermal properties with a dual-probe heat-pulse technique, *Soil Sci. Soc. Am. J.*, *58*, 1288–1294, 1994a.

Bristow, K. L., R. D. White, and G. J. Kluitenberg, Comparison of single and dual probes for measuring soil thermal properties with transient heating, *Aust. J. Soil Res.*, *32*, 447–464, 1994b.

Bristow, K. L., G. J. Kluitenberg, C. J. Goding, and T. S. Fitzgerald, A small multi-needle probe for measuring soil thermal properties, water content and electrical conductivity, *Comput. Electron. Agric.*, *31*, 265–280, 2001.

Campbell, G. S., *Soil Physics with BASIC — Transport models for soil-plant systems*, 150 pp., Elsevier Sci., New York, 1985.

Campbell, G. S., C. Calissendorff, and J. H. Williams, Probe for measuring soil specific heat using a heat pulse method, *Soil Sci. Soc. Am. J.*, *55*, 291–293, 1991.

Cass, A., G. S. Campbell, and T. L. Jones, Enhancement of thermal vapor diffusion in soil, *Soil Sci. Soc. Am. J.*, *48*, 25–32, 1984.

Chung, S.-O., and R. Horton, Soil heat and water flow with a partial surface mulch, *Water Resour. Res.*, *23*, 2175–2186, 1987.

De Marsily, G., *Quantitative Hydrogeology: Groundwater Hydrology for Engineers*, Academic, San Diego, Calif., 1986.

de Vries, D. A., Thermal properties of soils, in *Physics of Plant Environment*, edited by W. R. van Wijk, pp. 210–235, New York, North-Holland, 1963.

Gilmore, E., and J. S. Rogers, Heat units as a method of measuring maturity in corn, *Agron. J.*, *50*, 611–615, 1958.

Hopmans, J. W., and J. H. Dane, Thermal conductivity of two porous media as a function of water content, temperature, and density, *Soil Sci.*, *142*, 187–195, 1986a.

Hopmans, J. W., and J. H. Dane, Temperature dependence of soil hydraulic properties, *Soil Sci. Soc. Am. J.*, *50*, 4–9, 1986b.

Hopmans, J. W., J. M. N. Hendrickx, and J. S. Selker, Emerging measurement techniques for vadose zone characterization, in *Vadose Zone Hydrology: Cutting Across Disciplines*, edited by M. B. Parlange and J. W. Hopmans, pp. 279–316, Oxford Univ. Press, New York, 1999.

Hopmans, J. W., J. Šimunek, N. Romano, and W. Durner, Simultaneous determination of water transmission and retention properties — Inverse modeling of transient water flow, in *Methods of Soil Analysis, Part I*, 3rd ed., Monogr. 9, edited by G. C. Topp and J. H. Dane, in press, Am. Soc. of Agron., Madison, Wis., 2002.

Inoue, M., J. Šimunek, S. Shiozawa, and J. W. Hopmans, Simultaneous estimation of soil hydraulic and solute transport parameters from transient infiltration experiments, *Adv. Water Resour.*, *23*, 677–688, 2000.

Kay, B. D., and J. B. Goit, Temperature dependent specific heats of dry soil materials, *Can. Geotech. J.*, *12*, 209–212, 1975.

Kluitenberg, G. J., J. M. Ham, and K. L. Bristow, Error analysis of the heat-pulse method for measuring soil volumetric heat capacity, *Soil Sci. Soc. Am. J.*, *57*, 1444–1451, 1993.

Kluitenberg, G. J., K. L. Bristow, and B. S. Das, Error analysis of the heat pulse method for measuring soil heat capacity, diffusivity and conductivity, *Soil Sci. Soc. Am. J.*, *59*, 719–726, 1995.

Nassar, I. N., and R. Horton, Simultaneous transfer of heat, water, and solute in porous media, I, Theoretical development, *Soil Sci. Soc. Am. J.*, *56*, 1350–1356, 1992.

Noborio, K., K. J. McInnes, and J. L. Heilman, Measurements of soil water content, heat capacity, and thermal conductivity with a single TDR probe, *Soil Sci.*, *161*, 22–28, 1996.

Ren, T., K. Noborio, and R. Horton, Measuring soil water content, electrical conductivity and thermal properties with a thermo-TDR probe, *Soil Sci. Soc. Am. J.*, *63*, 450–457, 1999.

Ren, T., G. J. Kluitenberg, and R. Horton, Determining soil water flux and pore water velocity by a heat pulse technique, *Soil Sci. Soc. Am. J.*, *64*, 552–560, 2000.

Shiozawa, S., and M. Inoue, Solute dispersion in unsaturated unit-gradient water flow monitored in soil columns, *Soil Sci. Soc. Am. J.*, in press, 2001.

Šimunek, J., M. Šejna, and M. T. van Genuchten, The HYDRUS-2D software package for simulating two-dimensional movement of water, heat, and multiple solutes in variably-saturated media, version 2.0, *Rep. IGWMC-TPS-53*, 251 pp., Int. Ground Water Model. Cent., Colo. Sch. of Mines, Golden, 1999.

Sophocleous, M., Analysis of water and heat flow in unsaturated-saturated porous media, *Water Resour. Res.*, *15*, 1195–1206, 1979.

Tsang, Y. W., and K. Pruess, A study of thermally induced convection nears a high-level nuclear waste repository in partially saturated fractured tuff, *Water Resour. Res.*, *23*, 1958–1966, 1987.

Van Genuchten, M. T., A closed-form equation for predicting the hydraulic conductivity of unsaturated soils, *Soil Sci. Soc. Am. J.*, *44*, 892–898, 1980.

K. L. Bristow, CSIRO Land and Water, PMB Aitkenvale, Townsville, Queensland 4814, Australia. (Keith.Bristow@csiro.au)

J. W. Hopmans, Department of Land, Air and Water Resources, 123 Veihmeyer Hall, Davis, CA 95616-8628, USA. (jwhopmans@ucdavis.edu)

J. Šimunek George, E. Brown Jr. Salinity Laboratory, Agricultural Research Service, U.S. Department of Agriculture, 450 West Springs Road, Riverside, CA 92507-4617, USA. (JSIMUNEK@ussl.ars.usda.gov)